Correlation satellites in the photoelectron spectrum of argon

Wasantha Wijesundera and Hugh P. Kelly
Department of Physics, University of Virginia, Charlottesville, Virginia 22901
(Received 11 April 1988)

Many-body perturbation theory has been used to calculate photoionization cross sections with excitation of neutral argon from the single-ionization threshold at 15.76 to 100.00 eV. Resonance structure due to both single-electron excitations ($3s \rightarrow np$) and double-electron excitations ($3s^2 3p^6 \rightarrow 3s^2 3p^4 mn$) has been included. Calculated cross sections leaving the ion in $3s^2 3p^5$, $3s 3p^6$, $3s^2 3p^4(^1D)md(^2S)$, and $3s^2 3p^4 4p(^2P)$ levels are compared with experiment and previous calculations. Calculated cross sections for $3s^2 3p^6 \rightarrow 3s 3p^6 \epsilon p$ and $3s^2 3p \rightarrow 3s^2 3p^4 4p \epsilon d/\epsilon s$ excitations were used to determine the satellite intensities, which are compared with photoelectron measurements and other calculations. Results are also presented for the total cross section and the angular-asymmetry parameter for $3p$ electrons.

I. INTRODUCTION

In recent years there has been considerable interest in studying the satellite spectra of atoms,[1-4] which represent cross sections for photoionization with excitation. These cross sections are of great interest since they depend critically upon effects of electron correlations.

An extensive satellite spectrum has been observed[5-16] in argon following ionization in the $3s$ shell. The strong satellite lines which belong to the $3s^2 3p^4 md(^2S)$ series are of particular interest. It is now many years since Minnhagen[17] explained $3s^2 3p^4 md(^2S)$ satellites due to the strong interactions in the final ionic core states between the $3s 3p^6(^2S)$ level and the $3s^2 3p^4 md(^2S)$ series. This satellite spectrum has been observed by using photoelectron[5-11] (γ, e) and electron momentum[12-15] $(e, 2e)$ spectroscopic methods, and some disagreement exists between them as to the relative intensities of satellite lines. Inconsistencies also exist between different theoretical calculations[18-28] and were discussed in our recent work.[29]

Among other satellite lines, three "shakeup" satellite lines, $3s^2 3p^4(^3P)4p(^2P)$, $3s^2 3p^4(^1D)4p(^2P)$, and $3s^2 3p^4(^1S)4p(^2P)$, have been observed by Adam *et al.*,[6,7] Schmidt,[8] Kossmann *et al.*,[9] Svensson *et al.*,[10] and Silfvast *et al.*[30] The final ionic states corresponding to these three lines and the final ionic state $3s^2 3p^5(^2P)$ have the same angular momentum. Dyall and Larkins[21] calculated the relative intensities of the $3s^2 3p^4(^3P)4p(^2P)$, $3s^2 3p^4(^1D)4p(^2P)$, and $3s^2 3p^4(^1S)4p(^2P)$ satellites using configuration interaction among the final ionic states mentioned above.

In this paper we present a detailed calculation of the photoionization cross section with excitation of the neutral argon atom in the $3s^2 3p^6$ ground state for photon energies ranging from the single ionization threshold at 15.76–100.00 eV. The calculated partial cross sections include excitations leaving the ion in the levels $3s^2 3p^5$, $3s 3p^6$, $3s^2 3p^4\, md$, and $3s^2 3p^4 4p$ as listed in Table I. The relative intensities of satellites are obtained from ratios of the absolute cross sections. In a recent paper,[29] we presented the cross sections and the relative intensities for $3s^2 3p^6 \rightarrow 3s^2 3p^4 md$ excitations. In this paper the effects of resonances due to both $3s \rightarrow np$ excitations and $3s^2 3p^6 \rightarrow 3s^2 3p^4 mn$ excitations are included. The calculations were carried out in LS coupling. We used many-body perturbation theory (MBPT)[31-33] and our coupled equations method[34] to account for interactions between different channels in the final state. Since our final-state channels included those with single and double excitations, our calculations show both single-electron and double-electron resonance structure.

Section II includes the theoretical details of our method. We present results of calculations in Sec. III, and conclusions are contained in Sec. IV.

II. THEORY AND METHODS

In this work we use the dipole approximation for absorption of electromagnetic radiation and neglect spin-orbit splitting and relativistic effects. Atomic units are used throughout the paper.

The photoionization cross section in the dipole approx-

TABLE I. Threshold energies for excitations.

Channel	Experiment (eV)	ΔSCF (eV)[a]
$3s^2 3p^5(^2P)\epsilon d/\epsilon s$	15.76[b]	14.80
$3s 3p^6(^2S)\epsilon p$	29.24[b]	33.20
$3s^2 3p^4(^1D)3d(^2S)\epsilon p$	38.60[c]	38.96
$3s^2 3p^4(^1D)4d(^2S)\epsilon p$	41.21[c]	40.59
$3s^2 3p^4(^1D)5d(^2S)\epsilon p$	42.67[c]	41.45
$3s^2 3p^4(^3P)4p(^2P)\epsilon d/\epsilon s$	35.64[c]	38.31
$3s^2 3p^4(^1D)4p(^2P)\epsilon d/\epsilon s$	37.15[c]	39.14
$3s^2 3p^4(^1S)4p(^2P)\epsilon d/\epsilon s$	39.57[c]	41.54

[a] Threshold energies calculated by the difference between Hartree-Fock calculations of the ionic-core level and the ground state $3s^2 3p^6(^1S)$.
[b] Experimental values, Ref. 40.
[c] Experimental value, Ref. 10.

imation is given by

$$\sigma(\omega)=\frac{4\pi}{c}\omega\,\mathrm{Im}\alpha(\omega)\ , \tag{1}$$

where $\mathrm{Im}\alpha(\omega)$ is the imaginary part of the frequency-dependent dipole polarizability.[35,36]

The many-body perturbation theory (MBPT) expansion for $\alpha(\omega)$ can be derived[31,32,37] for an atom of charge Z described by the Hamiltonian

$$H=\sum_{i=1}^{N}T_i+\sum_{i<j=1}^{N}v_{ij}\ , \tag{2}$$

where T_i represents the kinetic energy operator for the ith electron and all one-body potentials acting on the ith electron. The term v_{ij} represents the Coulomb interaction between electrons i and j.

The Hamiltonian may be simplified by approximating the electron pair-interaction term $\sum_{i,j}v_{ij}$ by a sum of interactions with a single-particle potential V_i chosen to account for the average interaction of the ith electron with the remaining $N-1$ electrons. The Hamiltonian then becomes

$$H=H_0+H_c\ , \tag{3}$$

where

$$H_0=\sum_{i=1}^{N}(T_i+V_i)\ , \tag{4}$$

and

$$H_c=\sum_{i<j=1}^{N}V_{ij}-\sum_{i=1}^{N}V_i\ . \tag{5}$$

When the atom is exposed to an external electromagnetic radiation field $F\hat{\epsilon}_z\cos\omega t$, the resulting interaction is given in the dipole approximation by

$$V_{\mathrm{ext}}=F\cos\omega t\sum_{i=1}^{N}z_i\ . \tag{6}$$

Using time-dependent perturbation theory, $\mathrm{Im}\alpha(\omega)$ is given in terms of dipole matrix elements and matrix elements of the correlation interaction H_c. The length form of the many-body dipole matrix element is

$$Z_L=\left\langle\psi_f\left|\sum_{i=1}^{N}z_i\right|\psi_0\right\rangle\ , \tag{7}$$

where ψ_0 and ψ_f are exact many-electron initial and final states, respectively. The dipole velocity form is

$$Z_v=\frac{1}{E_0-E_k}\left\langle\psi_f\left|\sum_{i=1}^{N}\frac{d}{dz_i}\right|\psi_0\right\rangle\ , \tag{8}$$

where E_0 and E_f are energy eigenvalues corresponding to ψ_0 and ψ_f.

By use of many-body perturbation theory, the matrix element Z_L (Z_v) is obtained from an infinite series of open diagrams which have one dipole interaction and any number of interactions with the electron-correlation perturbation H_c given by Eq. (5) and leading to the final state.[37] Low-order perturbation diagrams contributing to Z_L (Z_v) for the transition $3p^6\rightarrow 3p^4rk$ are shown in Fig. 1. The symbol r represents a bound excited orbital, and k represents a continuum orbital. The exchange diagrams are not always shown but are understood to be included. In these diagrams a solid dot represents the dipole matrix element and a dashed line between two lines represents interaction with the correlation term H_c. Coulomb interactions with H_c below (above) the dipole interaction correspond to correlations in the initial (final) state. Figures 1(f) and 1(g) are second order in H_c. Diagrams contributing to Z_L (Z_v) for the transitions $p\rightarrow k$ involving a single excitation are not shown but were included. More details about these diagrams may be found in previous work.[38,39] Diagrams for single-excitation cross sections which contain double-electron resonances are shown in Fig. 2. Figures 2(a)–2(c) have a series of simple poles from energy denominators,

$$D_n=2\epsilon_{3p}-\epsilon_{k''}-\epsilon_{k'''}+\omega\ , \tag{9}$$

when the k'' and k''' states represent resonant bound states such as $3dnp$, $4pns$, $4pnd$, etc. These poles are broadened and shifted by summing higher order-contributions, as indicated in Fig. 2(d), to all orders by the use of our coupled equations method.[34] The coupled equations method is equivalent to the K matrix or close-coupling method discussed by Starace.[35] Resonances due to the diagrams shown in Fig. 2 appear in the $3p^5k$ cross section. Figure 1(g) also contributes to double-electron resonances when the r' and k'' states represent resonant bound double-excited states. These resonances appear in the $3p^4rk$ cross section, where r is a bound excited state.

The channels included in our calculation are given in Table I, along with photoionization threshold energies taken from experiment.[10,40] In Table I for comparison we also give our calculated threshold energies obtained by differences between Hartree-Fock[41] calculations for the ground state and the ionic levels (ΔSCF). Using experimental energies corresponds to a summation of higher-order terms in the perturbation expansion.[42] We did not include $2p\rightarrow\epsilon d/\epsilon s$ channels since a preliminary calculation indicated their effects on the $3s$ and $2p$ channels were small. We have included channels corresponding to all large satellites observed by Svensson *et al.*[10] at 1487 eV photon energy.

The $3s3p^6(^2S)$ orbitals were obtained from a Hartree-Fock (HF) calculation[41] and md orbitals of $3s^23p^4md(^2S)$ were evaluated by frozen-core HF calculations, with the core taken from a HF calculation for $3s^23p^4(^1D)$. All md orbitals are mutually orthogonal since they are calculated in the same potential. The configuration interaction calculation (CI) for $3s3p^6(^2S)$ and $3s^23p^4md(^2S)$ was performed by using 10 md orbitals ($m=3-12$) as described by Smid and Hansen[22] to account for the strong interaction between the $3s3p^6$ level and the $3s^23p^4(^1D)md$ series. The influence of the ϵd continuum in the CI calculation was not explicitly included but is roughly represented in the highest md orbital. The overlap integrals were included in calculating interaction between $3s3p^6$ and $3s^23p^4md$ states. The mixing coefficients were used to calculate appropriate potentials for bound and continuum states of $3s3p^6(^2S)\epsilon p$ and $3s^23p^4md(^2S)\epsilon p$.

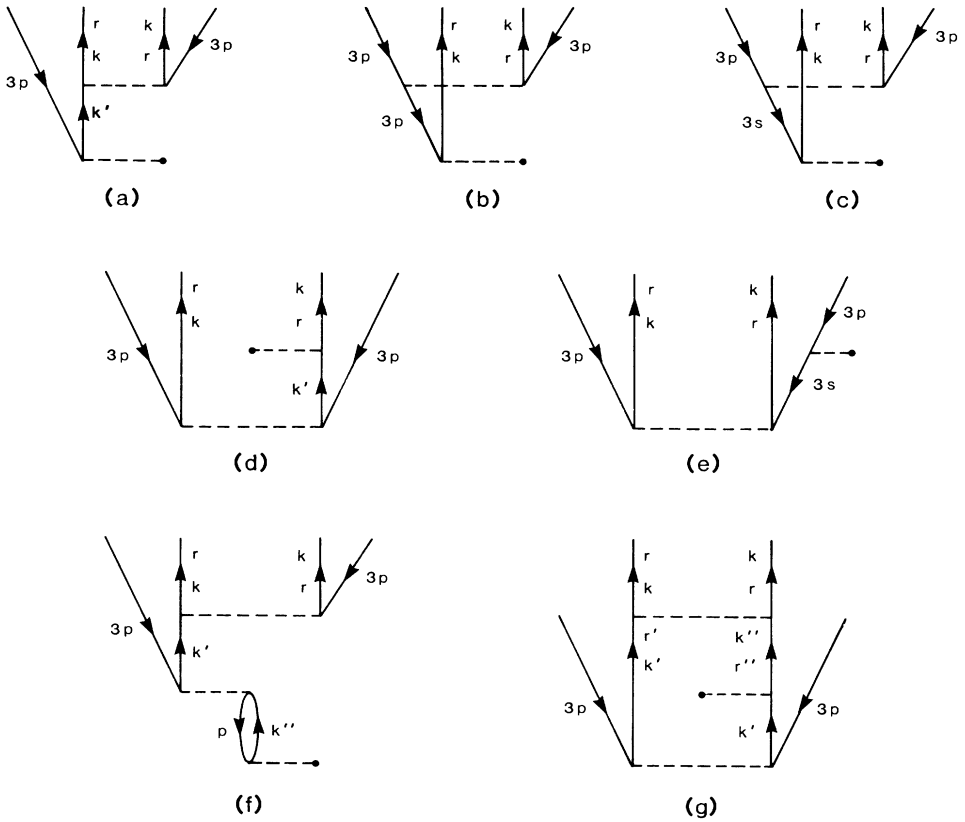

FIG. 1. Lowest-order diagrams which contribute to the dipole matrix elements of the transition $3s^2 3p^6 \rightarrow 3s^2 3p^4 rk$. Dashed lines ending with a solid dot indicate matrix elements of z. Other dashed lines represent Coulomb interactions. (a)–(c) Final-state correlations; (d) and (e) ground-state correlations; (f) and (g) coupling between final-state channels.

The symbol ϵ represents both bound and continuum states. The bound and continuum ϵd and ϵs states of $3s^2 3p^5(^2P)\epsilon d$ and $3s^2 3p^5(^2P)\epsilon s$ were calculated in Hartree-Fock[41] potentials. The same ϵd and ϵs states were used for the bound and continuum states of $3s^2 3p^4(^1D,^3P,^1S)4p(^2P)\epsilon d/\epsilon s$ states. The interaction between the $3s^2 3p^5(^2P)$ and $3s^2 3p^4 4p(^2P)$ ionic states were included in Fig. 1(b). Cross sections for other channels based on $3s^2 3p^4 4p$ are believed to be small.[30]

Our coupled equations method[34] was used to couple the interactions between single- and double-excitation channels to all orders in perturbation theory. We corrected ϵd (ϵs) wave functions used for $3s^2 3p^4(^1D,^3P,^1S)4p(^2P)\epsilon d$ (ϵs) by including the difference between the potentials appropriate for $3s^2 3p^4(^1D,^3P,^1S)4p(^2P)\epsilon d$ (ϵs) states and $3s^2 3p^5(^2P)\epsilon d$ (ϵs) states in the coupled equations. Calculated cross sections for $3s^2 3p^6 \rightarrow 3s 3p^6 \epsilon p$ excitations and for $3s^2 3p^6 \rightarrow 3s^2 3p^4$ $(^1D)md(^2S)\epsilon p$ and $3s^2 3p^4 4p(^2P)\epsilon d/\epsilon s$ excitations were used to determine the satellite intensities. The photoionization threshold energies were taken from experiment[10,40] for all excitations considered.

III. RESULTS

We present results in Fig. 3 for our calculated $3p$ partial cross section ($3p \rightarrow \epsilon d$ and $3p \rightarrow \epsilon s$) from threshold at

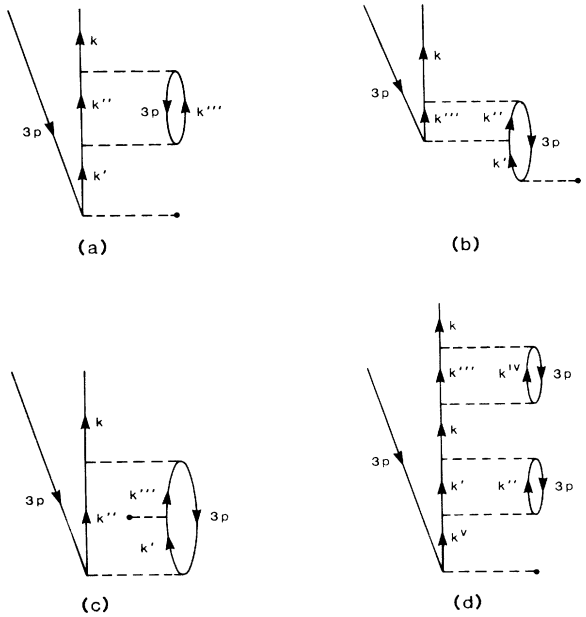

FIG. 2. Resonance diagrams involving doubly excited states. Symbols as in Fig. 1.

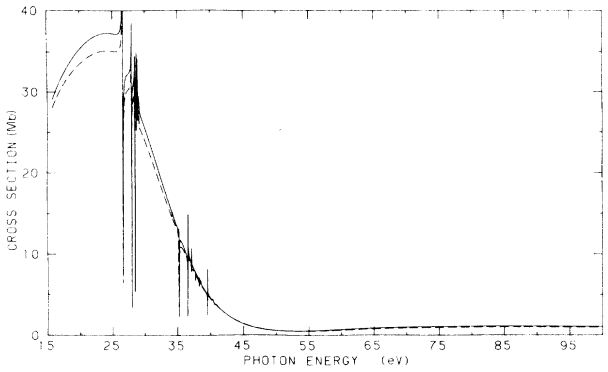

FIG. 3. $3p$ cross section, in dipole length (solid line) and dipole velocity (dashed line) formalism. The curves are the sum of $3p \rightarrow \epsilon d$ and $3p \rightarrow \epsilon s$ contributions. These curves were obtained by the coupled equations method including coupling with the photoionization with excitation channels.

15.76 to 100.00 eV in both length and velocity approximations. In the range 26.2–29.10 eV there are single-electron excitations $3s \rightarrow np$ which are degenerate with $3p \rightarrow \epsilon d$, ϵs excitations and give rise to resonances. The dominant resonances calculated in this range are $3s3p^6(^2S)4p$ at 26.2 eV, $3s3p^6(^2S)5p$ at 28.00 eV, and $3s3p^6(^2S)6p$ at 28.50 eV. The resonances corresponding to two-electron excitations $3p^2 \rightarrow mn$ lie between 35.24 and 40.70 eV. The resonance at 34.20 eV is $3s^23p^4(^3P)4p(^2P)5s$. Other large resonances are $3s^23p^4(^1D)4p(^2P)5s$ at 35.24 eV, $3s^23p^4(^1D)4d(^2S)4p$ at 36.56 eV, $3s^23p^4(^1D)5d(^2S)4p$ and $3s^23p^4(^1D)3d(^2S)5p$ at 37.10 eV, and $3s^23p^4(^1D)4d(^2S)5p$ at 39.51 eV. We have used this nomenclature since our calculated bound (continuum) states corresponding to two-electron excitations are based on channels such as $3s^23p^4(^1D)md(^2s)\epsilon p(^1P)$, etc., where ϵp refers to both bound states np ($n \geq 4$) and continuum states. As a result, we have a resonance state represented as $3s^23p^4(^1D)4d(^2S)4p(^1P)$ which differs from the usual coupling order. A more complete representation of this resonance would include admixtures with the $3s^23p^4(^1D)4d(^2P,^2D)4p(^1P)$ levels and there would then be three different $4d4p$ resonances. However, because of strong coupling of $3s^23p^4(^1D)4d(^2S)$ with the $3s3p^6(^2S)$ single-excitation level, we expect that the $3s^23p^4(^1D)4d(^2S)4p(^1P)$ description is appropriate for the largest of these three resonances. The cross section, which has a minimum at 53.00 eV, gradually increases and reaches a maximum near 84.0 eV.

Madden *et al.*[43] observed two-electron excitation resonances in the region between 27.0 and 40.0 eV including the resonances $3s^23p^4(^3P)4p(^2P)5s$ at 33.60 eV and $3s^23p^4(^1D)4p(^2P)5s$ at 35.26 eV. Our calculated positions for these resonances are 34.20 and 35.24 eV, respectively. The resonance $3s^23p^4(^1D)3d(^2S)4p$ does not appear in our calculated $3p$ cross section, in agreement with experimental observation.[43] The resonances $3s3p^4(^1D)4d(^2S)4p$, $3s^23p^4(^1D)5d(^2S)4p$, $3s^23p^4(^1D)3d(^2S)5p$, and $3s^23p^4(^1D)4d(^2S)5p$ which we calculated were not identified by Madden *et al.*[43]

The $3s \rightarrow np$ resonance structure in Fig. 3 does not agree as well with experiment[43] as that calculated previously in a low-order many-body calculation[44] in which corrections to the $3s \rightarrow np$ dipole matrix elements due to interaction with $3p \rightarrow \epsilon d, \epsilon s$ excitations and initial-state correlations were omitted. Including these correlations in the present calculation gives worse agreement with experiment. However, additional higher-order diagrams not included in this coupled equations calculation tend to restore good agreement with experiment.[45] Experimental results exist for the total cross section (including satellite channels) starting at the $3p$ threshold, and these will be compared with our calculated total cross section in a later figure.

We compare results of two different calculations for the $3p$ partial cross section in Fig. 4. The dashed line represents the $3p$ partial cross section in length form calculated including only the interactions between final-state channels in which there is a single excitation. The channels coupled were $3s^23p^5\epsilon d$, $3s^23p^5\epsilon s$, and $3s3p^6\epsilon p$. The full curve represents the $3p$ partial cross section in length form (also shown in Fig. 3) which includes interactions with single- and double-excitation channels. We notice a slight decrease in the $3p$ cross section once we include the interactions with double-excitation final-state channels. We interpret this as due to loss of flux from the $3p \rightarrow \epsilon d, \epsilon s$ channels to the photoionization with excitation channels.

We present our results for the $3s \rightarrow \epsilon p$ length and velocity cross sections from threshold at 29.24–100.00 eV in Fig. 5. The resonances are the same double-electron resonances as in the $3p$ cross section. The resonance at 34.20 eV is $3s^23p^4(^3P)4p(^2P)5s$. Other dominant resonances are $3s^23p^4(^1D)4p(^2P)5s$ at 35.24 eV, $3s^23p^4(^1D)4d(^2S)4p$ at 36.56 eV, $3s^23p^4(^1D)5d(^2S)4p$ and $3s^23p^4(^1D)3d(^2S)5p$ at 37.10 eV, and $3s^23p^4(^1D)4d(^2S)5p$ at 39.51 eV. The nomenclature of

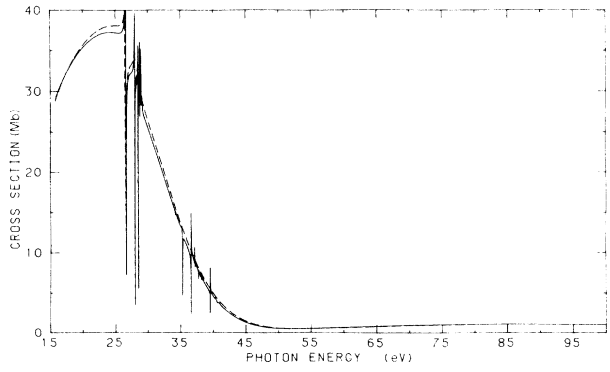

FIG. 4. Solid line represents the $3p$ cross section ($3p \rightarrow \epsilon d$ plus $3p \rightarrow \epsilon s$) in length form as shown in Fig. 3. The dashed line represents the $3p$ cross section in length form calculated by including only final-state channels in which there is a single excitation. The difference between the dashed curve and the solid curve is interpreted as loss of flux to the photoionization with excitation channels.

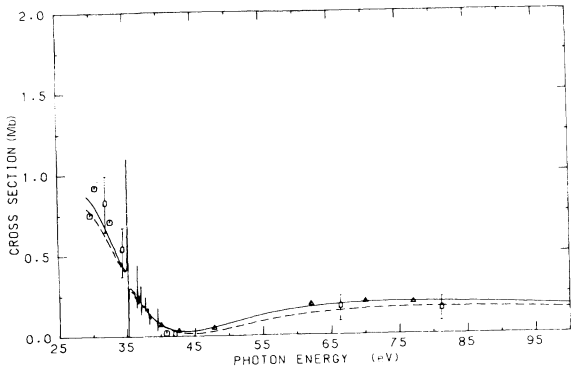

FIG. 5. Partial photoionization cross section calculated in dipole length (——) and dipole velocity (— — —) formalism for $3s^2 3p^6 \rightarrow 3s 3p^6 \epsilon p$. △, 3s cross section measured by Adam *et al.* (Ref. 7); ⊙, 3s cross section measured by Samson *et al.* (Ref. 46); ○, cross section measured by Houlgate *et al.* (Ref. 47).

the resonances was explained earlier in this section. The cross section has a Cooper minimum at 43.80 eV. Our calculated 3s cross section is in good agreement with experiment.[7,46,47] Our results agree with those calculated by Amusia *et al.*[48] except at the Cooper minimum where their calculated 3s cross section is zero. The nonzero value in our present calculation is due to the contribution to the 3s cross section from the imaginary part of the dipole matrix elements corresponding to the transition $3s \rightarrow \epsilon p$. However, the minima measured by Samson *et al.*[46] and by Houlgate *et al.*[47] are closer to zero than our calculated minimum.

In Fig. 6 our results for the $3s^2 3p^4(^1D) md(^2S) \epsilon p$

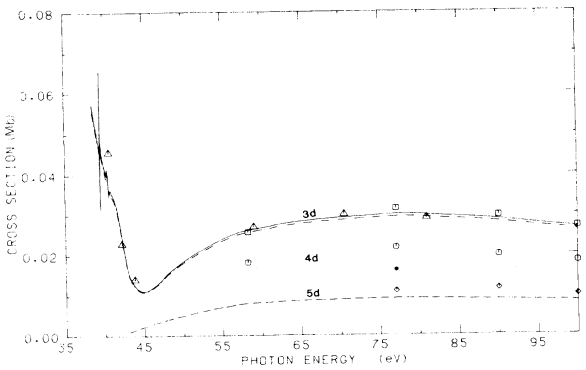

FIG. 6. Photoionization cross sections of $3s^2 3p^4(^1D) md(^2S)$ satellites. —— (—·—·—·) line is the cross section of the $3d(^2S)$ satellite in length (velocity) formalism. · · · · and — — — are the cross sections of $4d(^2S)$ and $5d(^2S)$ in the length formalism, respectively. ⚠, experimental cross section measured by Becker *et al.* (Ref. 49); ⊡, ⊙, and ◈ give the experimental cross sections of the $3d(^2S)$, $4d(^2S)$, and $5d(^2S)$ satellites. These experimental values were determined using the experimental relative intensities of Ref. 9 and our calculated 3s cross section. ●, $4d(^2S)$ cross section measured by Samson *et al.* (Ref. 11).

($m=3,4,5$) cross sections are presented and compared with experimental values. Our calculated results were presented in a previous article,[29] and we show them again to compare with recent experimental measurements.[11,49] The solid dot at 77 eV for the 4d cross section was obtained in the recent measurement by Samson *et al.*[11] By observing the fluorescence spectrum of the satellite lines Samson *et al.*[11] have shown that the previous measurement[9] of the $3p^4(^1D)4d(^2S)$ line in the photoelectron spectrum contains a contribution of approximately 25% from the $3p^4(^3P)5d(^2D,^2P)$ lines. We obtained the point represented by a solid dot by subtracting this contribution from the measurement by Kossmann *et al.*[9] at 77.0 eV photon energy. The result is in good agreement with our work and the calculation of Smid and Hansen.[24] The tabulated threshold energies for the $3s^2 3p^4(^1D) md(^2S)$ ($m=3,4,5$) satellites are given in Table I. For $3s^2 3p^4(^1D) 3d(^2S)$ channel both length and velocity cross sections are shown in Fig. 6 and are in close agreement. The resonance at 39.51 eV is $3s^2 3p^4(^1D) 4d(^2S) 5p$. Other resonances shown are the higher members of the Rydberg series of $3s^2 3p^4 4d(^2S) np$ and $3s^2 3p^4 5d(^2S) np$. The cross section has a minimum at 45.00 eV, gradually increases, and then begins to decrease slightly. This behavior agrees with experimental observations by Adam *et al.*[6] Since velocity and length results are very close for the $3s^2 3p^4(^1D) 4d(^2S) \epsilon p$ and $3s^2 3p^4(^1D) 5d(^2S) \epsilon p$ cross sections, only length forms are shown. Our calculated cross sections for the satellites decrease with increasing principal quantum number (m) of the md series as expected and as observed in experiments.[7,10] The calculated cross sections of Fig. 6 do not include effects of relaxation and polarization and are probably less accurate within 5.0 eV of threshold than at higher energies.

As pointed out previously by Adam *et al.*,[7] the shape of the $3d(^2S)$ cross section is very similar to that of the $3s 3p^6(^2S)$ cross section.[7,46,47] This is interpreted[29,49] as due to the fact that the coupling with the $3s 3p^6 \epsilon p$ channel is driving the $3d(^2S) \epsilon p$ channel. It is also interesting to note the strong effects on the $3s 3p^6 \epsilon p$ channel due to coupling with the $3s^2 3p^5 \epsilon d / \epsilon s$ channels.[35] We believe that the $4d(^2S)$ and $5d(^2S)$ cross sections would also show the characteristic shape of the $3s 3p^6(^2S)$ cross section if the oscillator strengths were extended into the region of bound Rydberg states. Very close to threshold in the $4d(^2S)$ cross section there are $3s^2 3p^4(^1D) 5d(^2S) np(^1P)$ resonances due to high-lying np Rydberg states, but these are not shown. There should also be resonance structure in the $5d(^2S)$ cross section, but we did not obtain this structure because we did not include the $6d(^2S)$ channel and channels of higher excitation.

The calculated relative intensities for the $3p^4(^1D) md(^2S)$ satellites, which include the effects of ground-state and final-state correlations, were presented in a previous paper,[29] and our results were shown to be in reasonable agreement with photoionization experiments.[5-7,9,10] The relative intensity for a given satellite is the ratio of the cross section of the satellite to the cross section of the 3s line, in percent.

We show our results for the $3s^2 3p^4(^3P) 4P(^2P)$ cross

sections [sum of $3s^2 3p^4(^3P)4p(^2P)\epsilon d$ and $3s^2 3p^4(^3P)4p(^2P)\epsilon s$ cross sections] in both length and velocity forms in Fig. 7. The dominant resonances shown in the range 35.64–40.70 eV are $3s^2 3p^4(^1D)4d(^2S)4p$ at 36.56 eV, $3s^2 3p^4(^1D)5d(^2S)4p$ and $3s^2 3p^4(^1D)3d(^2S)5p$ at 37.10 eV, and $3s^2 3p^4(^1D)4d(^2S)5p$ at 39.51 eV. These resonances also appear in the cross sections shown in the previous figures. The nomenclature of resonances was explained earlier in this section. Our calculated cross section (solid line for length and dashed line for velocity) reaches a maximum value at 43.00 eV, gradually decreases, and then increases to a broad second maximum at higher energies. The dot-dash curve represents the cross section calculated by Silfvast *et al.*,[30] who used the computer code of Cowan[50] to calculate relativistic Hartree-Fock wave functions and to perform configuration interaction (CI) calculations including both initial-state configuration (ISCI) and final ionic-core state configuration (FISCI) interactions. The "experimental" results at low energies were deduced by Silfvast *et al.*[30] from the total cross section for the sum of four satellites (Nos. 1, 2, 3, and 4′) from Adam *et al.*[7] and the relative intensity of satellite No. 2 measured by Adam *et al.*[7] Adam *et al.*[7] have tentatively assigned their satellite No. 2 to either the $3s^2 3p^4(^3P)4p(^2P)$ or $3s^2 3p^4(^3P)4p(^2D)$ which are very close. Silfvast *et al.*[30] have compared the sum of their calculated cross sections for these two satellites to the "experimental" cross section corresponding to the satellite No. 2 of Adam *et al.*[7] We have also assumed that this measured satellite cross section is the sum of the $3p^4(^3P)4p(^2P)$ and $3p^4(^3P)4p(^2D)$ cross sections. We then used the ratio between the population densities (neglecting the energy dependence of the population density) of these two satellites as observed by Silfvast *et al.*[30] and the above experimental results to estimate the cross section of the $3p^4(^3P)4p(^2P)$ satellite at low energies. We recognize that the experimental points obtained this way are tentative. They are shown in Fig. 7 as crosses. The experimental values given in the range 77.00–100.00 eV were obtained using our calculated 3*s* cross section and the relative intensities measured by Kossmann *et al.*[9]

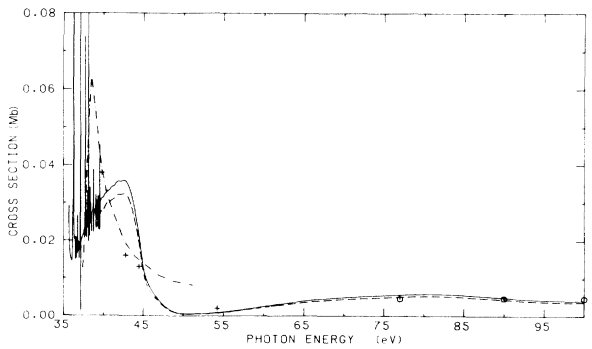

FIG. 7. Photoionization cross section of the $3s^2 3p^4(^3P)4p(^2P)$ satellite in dipole length (——) and dipole velocity (— — —) formalism. —·—·—·, $3s^2 3p^4(^3P)4p(^2P)$ cross section calculated by Silfvast *et al.* (Ref. 30); +, cross section deduced by Silfvast *et al.* (Ref. 30), from measurement by Adam *et al.* (Ref. 7); ⊙, experimental values determined using the experimental relative intensities of Ref. 9 and our calculated 3*s* cross section.

In Fig. 8 we present our results for the $3s^2 3p^4(^1D)4p(^2P)$ cross section [sum of $3s^2 3p^4(^1D)4p(^2P)\epsilon d$ and $3s^2 3p^4(^1D)4p(^2P)\epsilon s$ cross sections] in both length and velocity forms. The resonances present in the dense region of Rydberg resonances are the higher members of the $3s^2 3p^4(^1D)mdnp$ ($m=3,4,5$) and $3s^2 3p^4(^1S)4pnd/ns$ ($n>5$) series. The dot-dash curve represents the cross section calculated by Silfvast *et al.*[30] Adam *et al.*[7] have tentatively assigned their satellite No. 3 to either the $3p^4(^1D)4p(^2P)$ or $3p^4(^1D)3d(^2D)$. Since the $3p^4(^1D)3d(^2D)$ cross section was not calculated in this work, we are unable to make a comparison of our results for the $3p^4(^1D)4p(^2P)$ cross section with experiment.

The partial cross sections $3s^2 3p^4(^1S)4p(^2P)\epsilon d$ and $3s^2 3p^4(^1S)4p(^2P)\epsilon s$ were added to obtain the $3s^2 3p^4(^1S)4p(^2P)$ cross section shown in Fig. 9. The resonances shown near threshold are the higher members of the Rydberg series $3s^2 3p^4(^1D)4d(^2S)np$ ($n>5$) and $3s^2 3p^4(^1D)5d(^2S)np$ ($n>4$). The dot-dash curve represents the cross section calculated by Silfvast *et al.*[30] The experimental values given in the range 77.00–100.00 eV were obtained using our calculated 3*s* cross section and the relative intensities measured by Kossmann *et al.*[9] The $3s^2 3p^4(^1S)4p(^2P)$ cross section was observed at high photon energies[9] but not at low photon energies.[7] Our calculated cross section is quite small near threshold and is consistent with the experiment of Adam *et al.*[7] on which it was not observed at low energies.

In our calculation the ground- (initial-) state correlations for the $3s^2 3p^4\epsilon d/\epsilon s$ cross sections were calculated by evaluating Figs. 1(d) and 1(e). Our coupled equations method[34] was used to account for final-state interactions between the $3p^4 4p\epsilon d/\epsilon s$ channels and other channels given in Table I. The lowest-order diagrams contributing to the final-state correlations are shown in Figs. 1(a)–1(c). Figure 1(d) with $r=4p$ on the left, $k=\epsilon d$ on the right, and $k'=\epsilon' p$ gives the largest contribution to the ground-state correlations for the $3p^4 p\epsilon d/\epsilon s$ cross sections. The

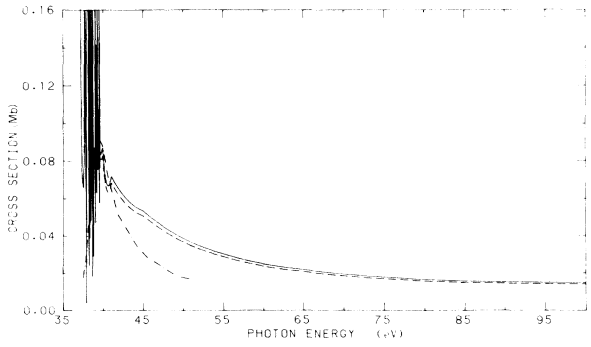

FIG. 8. Photoionization cross section of the $3s^2 3p^4(^1D)4p(^2P)$ satellite in dipole length (——) and dipole velocity (— — —) formalism. —·—·—·, cross section calculated by Silfvast *et al.* (Ref. 30).

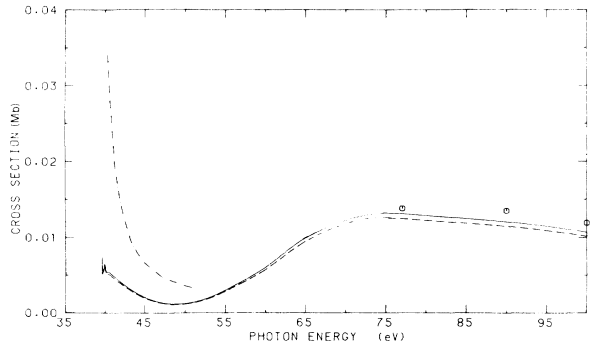

FIG. 9. Photoionization cross section of the $3s^2 3p^4(^1S)4p(^2P)$ satellite in dipole length (——) and dipole velocity (— — —) formalism. —·—·—·, cross section calculated by Silfvast *et al.* (Ref. 30); ⊙, experimental values determined using the experimental relative intensities of Ref. 9 and our calculated $3s$ cross section.

symbol ϵ' represents both bound and continuum states. Figure 1(d) with $k=\epsilon d$ on the left, $r=4p$ on the right, and $k'=\epsilon' d$ is approximately 40% of Fig. 1(d) with $r=4p$ on the left, $k=\epsilon d$ on the right, and $k'=\epsilon' d$. It is also of opposite sign. The contribution from Fig. 1(e) is small relative to that from Fig. 1(d). When the $3p^4 4p\epsilon d/\epsilon s$ cross sections were calculated including only ground-state correlations [Figs. 1 (d) and 1(e)], we obtain cross sections which were approximately 35% as large as our final cross sections which included both the final-state correlations and the ground-state correlations of Figs. 1(d)–1(e). Our final cross sections included final-state correlations to all orders among the channels given in Table I. We also found that the $3p^4 4p\epsilon s$ cross sections are much smaller than the $3p^4 4p\epsilon d$ cross sections.

The calculated relative intensities for $3s^2 3p^4 4p$ satellites are given in Table II at photon energies for which measured or previously calculated values exist. Since our length and velocity results are very close, only the length results are shown. Our relative intensity for a given satellite is the ratio of the cross section of the satellite to the cross section of the $3s$ line, in percent. Experimental values are taken from Refs. 9 and 10. The calculated values of Dyall and Larkins[21] are also given. Our calculated relative intensities for the $3s^2 3p^4 4p$ satellites agree reasonably with their calculations at 151.0 eV for the $(^3P)4p$ and $(^1D)4p$ cross sections but disagree significantly for the $(^1S)4p$ cross section. At the photon energy 1487.0 eV, our results are much higher than those of Dyall and Larkins[21] for all three cross sections.

In Fig. 10 we present the total cross section which is the sum of all the calculated partial cross sections ($3p$, $3s$, and the satellites). We found that the ratio of the contribution from the sum of the cross sections of satellites we calculated to the total cross section is approximately 10% at 40.0 eV. However, this ratio varies as the $3p$ cross section varies with the photon energy. The resonances are the same as shown in Fig. 3. The agreement between the calculated and the experimental[43,51] cross section is very good. Our calculated results agree well with previous calculations[44] except near the $3s$-np resonances, as discussed earlier in this section.

In Fig. 11 we present the angular asymmetry parameter β in length form for the total $3p$ cross section. Since length and velocity results are very close, only the length result is shown. Our result for the β parameter agrees well with both experimental[47] and previously calculated[48] results. The resonance structure appearing between 26.62 and 29.10 is due to $3s\rightarrow np$ excitations. The β parameter also shows resonance structure due to two-electron excitations, $3s^2 3p^6\rightarrow 3s^2 3p^4 mn$ in the range 34.20–40.70 eV.

IV. DISCUSSION AND CONCLUSIONS

We have used many-body theory to calculate the photoionization cross sections for argon, leaving Ar^+ in $md(^2S)$ ($m=3,45$) and $4p(^2P)$ levels, including resonance structure due to single- and double-electron excitations. There is good agreement between length and velocity calculations.

We have compared the calculated $3s^2 3p^4(^1D)md(^2S)\epsilon p$ ($m=3,4,5$) cross sections with experimental values.[9,49] Experimental values of Kossmann *et al.*[9] were determined from our $3s$ cross section and their experimental relative intensities. Our $3d(^2S)$ cross section is in good

TABLE II. $3s^2 3p^4 4p$ satellite intensities relative to the $3s$ line (in percent). Error bars on the last significant number of each value are given in parentheses.

Energy	$3p^4(^3P)4p\,^2P$		$3p^4(^1D)4p\,^2P$		$3p^4(^1S)4p\,^2P$	
(eV)	Expt.	Calc.	Expt.	Calc.	Expt.	Calc.
77	2.3(6)[a]	2.8[b]		8.6[b]	6.9(6)[a]	6.5[b]
90	2.5(6)[a]	2.6[b]		8.2[b]	7.7(8)[a]	6.3[b]
100	2.7(6)[a]	2.4[b]		8.1[b]	6.9(8)[a]	6.1[b]
110	2.5(6)[a]	2.2[b]		7.9[b]	7.0(8)[a]	6.0[b]
120	2.1(6)[a]	1.9[b]		7.6[b]	6.3(6)[a]	5.8[b]
151		1.3[b], 1.1[c]		7.0[b], 6.6[c]		5.3[b], 1.6[c]
1487	0.6(1)[d]	0.8[b], 0.3[c]	3.7(3)[d]	4.1[b], 1.8[c]	1.5(2)[d]	1.9[b], 0.4[c]

[a] Reference 9.
[b] This work. Since length and velocity results are very close, only the length results are given.
[c] Reference 21.
[d] Reference 10.

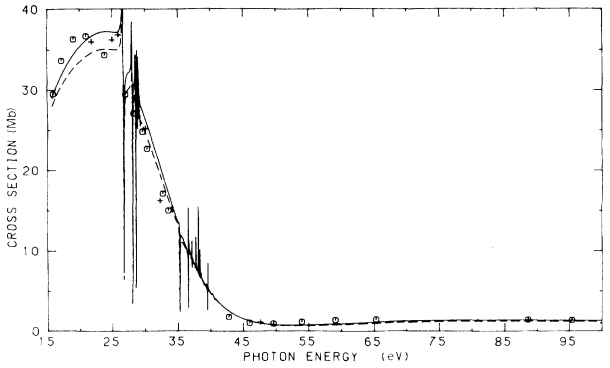

FIG. 10. The correlated total cross section in dipole length (——) and dipole velocity (— — —) formalism. ⊙, experimental values (Ref. 51); +, experimental values (Ref. 43). The calculated total cross section is the sum of all partial cross sections including the satellite channels.

agreement with experiments by Kossmann *et al.*[9] and Becker *et al.*[49] In the $4d(^2S)$ case, the experimental measurements by Kossmann *et al.*[9] are higher than our calculated results. Recently, Samson *et al.*[11] have shown that the measurement by Kossmann *et al.*[9] of the $3p^4(^1D)4d(^2S)$ satellite line in the photoelectron spectrum at 77.0 eV contains a contribution of approximately 25% from the $3s^23p^4(^3P)5d(^2D,^2P)$ lines. Subtracting this contribution from the experimental measurement by Kossmann *et al.*[9] at 77.0 eV photon energy brings their result into good agreement with our work and the calculations of Smid and Hansen.[24] Our calculated $5d(^2S)$ cross section also agrees reasonably with experiment,[9] although it is somewhat lower. The calculated cross sections were used to determine relative intensities of the $md(^2S)$ satellites relative to the $3s3p^6(^2S)$ main line. We found that there is strong interaction in the final ionic states between the $3s3p^6$ and $3s^23p^4(^1D)md(^2S)$ series, in agreement with experiments[5–16] and previous calculations.[18–28] We also found that the inclusion of initial-state correlations reduced our discrepancy between length and velocity cross sections by moving the velocity results closer to length results and there is only a slight influence of initial-state correlations on the relative intensities.

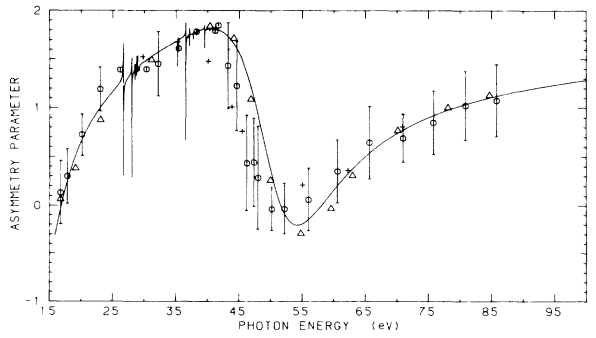

FIG. 11. Angular asymmetry parameter β for $3s^23p \rightarrow 3s^23p^5\epsilon d$, ϵs excitations in the length formalism. △, Amusia *et al.* (Ref. 48); ⊙, Houlgate *et al.* (Ref. 47); +, Adam *et al.* (Ref. 7).

Smid and Hansen[24] performed a configuration interaction calculation for the $3s3p^6$ and $3s^23p^4(^1D)md$ states including both bound and continuum md orbitals. They used mixing coefficients and the lowest-order $3s$ dipole matrix elements with the continuum ϵp to determine dipole matrix elements for the $3p^4md$ satellites given by Fig. 1(c) with $k=\epsilon p$ on the left and $r=md$ on the right. They calculated the ratio of the squared dipole matrix element for a given $3p^4md$ satellite line at a given photon energy to that of the $3s$ line. This ratio was taken as the relative intensity for a given satellite at a given photon energy, and their results are in good agreement with experiment.[7,9] A recent calculation by Hibbert and Hansen[26] includes extensive configuration interaction effects and is in good agreement with the experiment by Svensson *et al.*[10] at 1487 eV but differs somewhat from their earlier calculations.[23] Our calculated relative intensities of the $3p^4md$ satellites agree with those of Smid and Hansen[24] within a few percent but not as well with the recent extensive configuration interaction calculations of Hibbert and Hansen.[26]

We have also compared our calculated $3p^44p(^2P)\epsilon d/\epsilon s$ cross sections with those given by Silfvast *et al.*[30] in the photon energy range 35.0–50.0 eV. Silfvast *et al.*[30] calculated the contribution of initial-state correlations for the $3p^44p\epsilon d/\epsilon s$ cross sections using configuration interaction among $3p^63p^54p$, $3p^44p4f$, and $3p^44p^2$ states. In our calculation the initial-state correlations were calculated by evaluating the many-body diagrams of Figs. 1(d) and 1(e). We found that Fig. 1(d) with $k=\epsilon d$ on the left, $r=4p$ on the right, and $k'=\epsilon' d$ (a configuration not included by Silfvast *et al.*[30]) is 40% of Fig. 1(d) with $r=4p$ on the left, $k=\epsilon d$ on the right, and $k'=\epsilon' p$ and of opposite sign. Silfvast *et al.*[30] obtained their final ionic-state configuration interaction contribution by calculating the dipole transition probability of $3p^6 \rightarrow 3p^54s/3d$ and the configuration interaction of $3p^54s/3d$ with $3p^44p\epsilon s/\epsilon d$ continua. This is equivalent to the evaluation of the diagram of Fig. 1(a) with $r=4p$, $k=\epsilon d/\epsilon s$, and $k'=4s/3d$ and higher-order diagrams among the states considered by Silfvast *et al.*[30] However, one should include all $3p \rightarrow \epsilon' d/\epsilon' s$ (both bound and continuum states) excitations as we have done. This will increase the final-state correlation contribution above those found by Silfvast *et al.*[30] In our calculation the coupled equations method[34] was used to account for final-state interactions between the $3p^44p\epsilon d/\epsilon s$ channels and the other channels given in Table I.

Silfvast *et al.*[30] found that initial-state configuration interaction was the dominant correlation process. They also found that the contribution of final-state continuum ϵs electrons was much smaller than that of final ϵd electrons. When our $3p^44p\epsilon d/\epsilon s$ cross sections were calculated including only initial-state correlations [Figs. 1(d) and 1(e)], we obtained cross sections which were approximately only 35% as large as our final cross sections

which included both final-state and initial-state correlations. Therefore, we conclude that both initial- and final-state correlations are important. We also found that the $3p^4 4p\epsilon s$ cross sections are much smaller than the $3p^4 4p\epsilon d$ cross sections, in agreement with Silfvast *et al.*[30]

Our calculated $3p^4(^3P)4p$ cross section is not in close agreement with that given by Silfvast *et al.*[30] in the photon energy range 35.0–50.0 eV. Their results agree well with the tentative experimental values in the energy range 40.0–45.0 eV. At 54.8 eV their result, if extrapolated, seems unlikely to agree with experiment. Our results are in good agreement with experiment at 45.0 and 54.8 eV but not at 40.0 and 43.0 eV. At energies above 77.0 eV, our calculated $3p^4(^3P)4p$ cross section also agrees reasonably with the experimental[9] values. In Sec. III we explained how experimental values were obtained in the energy ranges 40.0–55.0 eV and 77.0–100.0 eV.

Our calculated $3p^4(^1D)4p(^2P)$ cross section is larger than that of Silfvast *et al.*[30] in the photon energy range 35.0–50.0 eV. Adam *et al.*[7] have measured relative intensities in this energy range and were uncertain as to whether they were observing the $3p^4(^1D)4p(^2P)$ or the $3p^4(^1D)3d(^2D)$ satellite. We have deduced the cross section for the satellite of Adam *et al.*[7] using their relative intensities and our calculated $3s$ cross section, and it does agree well with our calculated $3p^4(^1D)4p(^2P)$ cross section in the energy range 35.0–50.0 eV. However, because of the uncertainty about the $3p^4(^1D)3d(^2D)$ satellite, we have not shown the experimental cross section. It would be very useful to have both the experimental and theoretical cross sections of the $3p^4(^1D)3d(^2D)$ satellite, and we plan to calculate the $3p^4(^1D)3d(^2D)$ cross section in the near future.

The relative intensity of the $3p^4(^1D)4p(^2P)$ satellite has been measured at 1487.0 eV by Svenson *et al.*, and it is in reasonable agreement with our result shown in Table II. Svensson *et al.*[10] did not observe the $3p^4(^1D)3d(^2D)$ satellite in their spectrum at 1487 eV.

Our calculated $3p^4(^1S)4p(^2P)$ cross section is very small near threshold and is consistent with the experiment by Adam *et al.*[7] in which the $3p^4(^1S)4p(^2P)$ satellite was not observed. Our results are in close agreement with experiment[9] in the energy range 77.0–100 eV.

Dyall and Larkins[21] have used multiconfiguration shake theory[21,52,53] to calculate relative intensities of the $3p^4 4p$ satellites of Ar. They performed a configuration interaction calculation between $3s^2 3p^5$, $3s^2 3p^4 np$ ($n=4$–7), and $3s^2 3p^4 nf$ ($n=4,5$) configurations to obtain the multiconfiguration final state. The initial state was taken to be the single-configuration state $3s^2 3p^6$. Dyall and Larkins[21] pointed out that this model is only applicable in the high-photon-energy region where both interchannel coupling and the variation of the dipole interaction with energy may be neglected. Our results, at photon energy 1487.0 eV, are much higher than those of Dyall and Larkins.[21]

We performed two different calculations for the $3p$ partial cross section, one including only the interactions between final-state channels in which there is a single excitation and the other including interactions with both single- and double-excitation channels. We notice a slight decrease in the $3p$ cross section when we include the interactions with double-excitation final-state channels. We interpret this as due to loss of flux from $3p \rightarrow \epsilon d, \epsilon s$ channels to the photoionization with excitation channels.

We have also calculated the total cross section, which agrees reasonably with experiment.[43,51] Our calculated angular asymmetry parameter for the total $3p$ cross section shows resonance structure due to both single- and double-electron excitations. The results agree with experimental[7,47] and previously calculated results,[48] although the experiments[7,47] do not show the resonance structure.

We have found many-body perturbation theory (MBPT) to be useful in calculating cross sections of photoionization with excitation. We have observed that there is considerable cancellation among different amplitudes (diagrams) due to both initial- and final-state correlations. In these calculations it is only possible to include a limited number of excited configurations, and there can be considerable discrepancy between different calculations as in the case of calcium.[54–57] We have included many of the correlation effects in our calculation, but still cannot claim high accuracy. Therefore, it would be desirable to have more calculations using different methods and also experimental measurements for cross sections of photoionization with excitation.

ACKNOWLEDGMENTS

We thank the U.S. National Science Foundation for support of this work. We are also grateful to the Pittsburgh Supercomputer Center for a generous grant of computing time. We thank Cheng Pan, Daniel Frye, Mickey Kutzner, and Zikri Altun for helpful discussions. We also thank Professor J. A. R. Samson for a copy of his fluorescence results prior to publication for *md* satellites and for a useful discussion.

[1] A. Fahlman, M. O. Krause, and T. A. Carlson, J. Phys. B **17**, 1217 (1984).
[2] H. Derenbach and V. Schmidt, J. Phys. B **17**, 83 (1984).
[3] P. H. Kobrin, S. Southworth, C. M. Truesdale, D. W. Lindle, U. Becker, and D. A. Shirley, Phys. Rev. A **29**, 194 (1984).
[4] H. Schroder, B. Sonntag, H. Voss, and H. E. Wetzel, J. Phys. B **17**, 707 (1984).
[5] D. P. Spears, H. J. Fischbeck, and T. A. Carlson, Phys. Rev. A **9**, 1603 (1974).
[6] M. Y. Adam, F. Wuilleumier, S. Krummacher, V. Schmidt, and W. Mehlhorn, J. Phys. B **11**, L413 (1978).
[7] M. Y. Adam, P. Morin, and G. Wendin, Phys. Rev. A **31**, 1426 (1985).
[8] V. Schmidt, Z. Phys. D **2**, 275 (1986).
[9] H. Kossmann, B. Krassig, V. Schmidt, and J. E. Hansen, Phys. Rev. Lett. **58**, 1620 (1987).
[10] S. Svensson, K. Helenelund, and U. Gelius, Phys. Rev. Lett. **58**, 1624 (1987).

[11]J. A. R. Samson, Y. Chung, and E. Lee, Phys. Lett. A **127**, 171 (1988).
[12]I. E. McCarthy and E. Weigold, Phys. Rep. **27C**, 275 (1976).
[13]K. T. Leung and C. E. Brion, Chem. Phys. **82**, 87 (1983).
[14]I. E. McCarthy and E. Weigold, Phys. Rev. A **31**, 160 (1985).
[15]J. P. O. Cook, I. E. McCarthy, J. Mitroy, and E. Weigold, Phys. Rev. A **33**, 211 (1986).
[16]C. E. Brion, K. H. Tan, and G. M. Brancroft, Phys. Rev. Lett. **56**, 584 (1986).
[17]L. Minnhagen, Ark. Fys. **25**, 203 (1963).
[18]R. L. Martin, S. P. Kowalczyk, and D. A. Shirley, J. Chem. Phys. **68**, 3829 (1978).
[19]I. E. McCarthy, P. Uylings, and R. Poppe, J. Phys. B **11**, 3299 (1978).
[20]G. R. J. Williams, J. Electron Spectrosc. Relat. Phenom. **15**, 247 (1979).
[21]K. G. Dyall and F. P. Larkins, J. Phys. B **15**, 219 (1982).
[22]H. Smid and J. E. Hansen, J. Phys. B **14**, L811 (1981).
[23]H. Smid and J. E. Hansen, J. Phys. B **16**, 3339 (1983).
[24]H. Smid and J. E. Hansen, Phys. Rev. Lett. **52**, 2138 (1984).
[25]H. Smid and J. E. Hansen, J. Phys. B **14**, L97 (1985).
[26]A. Hibbert and J. E. Hansen, J. Phys. B **20**, L245 (1987).
[27]J. Mitroy, K. Amos, and I. Morrison, J. Phys. B **17**, 1659 (1984).
[28]M. Ya. Amusia and A. S. Kheifets, J. Phys. B **18**, L679 (1985).
[29]W. Wijesundera and H. P. Kelly, Phys. Rev. A **36**, 4539 (1987).
[30]W. T. Silfvast, D. Y. Al-Salameh, and O. R. Wood II, Phys. Rev. A **34**, 5164 (1986).
[31]K. A. Brueckner, Phys. Rev. **97**, 1353 (1955).
[32]J. Goldstone, Proc. R. Soc. London, Ser. A **239**, 267 (1957).
[33]H. P. Kelly, Adv. Theor. Phys. **2**, 75 (1968).
[34]E. R. Brown, S. L. Carter, and H. P. Kelly, Phys. Rev. A **21**, 1237 (1980).
[35]A. F. Starace, in *Theory of Atomic Photoionization,* Vol. XXXI of *Handbuch der Physik,* edited by S. Flügge and W. Mehlhorn (Springer-Verlag, Berlin, 1982), p. 1.
[36]U. Fano and J. W. Cooper, Rev. Mod. Phys. **40**, 441 (1968).
[37]H. P. Kelly, in *Photoionization and Other Probes of Many-Electron Interactions,* edited by F. Wuilleumier (Plenum, New York, 1976), p. 83.
[38]E. M. Isenberg, S. L. Carter, H. P. Kelly, and S. Salomonson, Phys. Rev. A **32**, 1472 (1985).
[39]W. Wijesundera and H. P. Kelly, Phys. Rev. A **36**, 3187 (1987).
[40]C. E. Moore, *Atomic Energy Levels,* Natl. Bur. Stand. (U.S.) Circ. No. 467 (U.S. GPO, Washington, D.C., 1949).
[41]C. F. Fischer, Comput. Phys. Commun. **4**, 107 (1972).
[42]H. P. Kelly and A. Ron, Phys. Rev. A **5**, 168 (1972).
[43]R. P. Madden, D. L. Ederer, and K. Codling, Phys. Rev. **177**, 136 (1969).
[44]H. P. Kelly and R. L. Simons, Phys. Rev. Lett. **30**, 529 (1973).
[45]E. R. Brown, Ph.D. thesis, University of Virginia, 1981.
[46]J. A. R. Samson and J. L. Gardner, Phys. Rev. Lett. **33**, 671 (1974).
[47]R. G. Houlgate, J. B. West, K. Codling, and G. V. Marr, J. Phys. B **7**, L470 (1974).
[48]M. Y. Amusia, N. A. Cherepkov, and L. V. Chernysheva, Phys. Lett. **A40**, 15 (1972).
[49]U. Becker, B. Langer, H. G. Kerkhoff, M. Kupsch, D. Szostak, R. Wehlitz, P. A. Heiman, S. H. Liu, D. W. Lindle, T. A. Ferrett, and D. A. Shirley, Phys. Rev. Lett. **60**, 1490 (1988).
[50]R. D. Cowan, *Theory of Atomic Structure and Spectra* (University of California Press, Berkeley, 1981), Secs. 8-1 and 16-1.
[51]G. V. Marr and J. B. West, At. Data **18**, 497 (1976).
[52]T. Aberg, Phys. Rev. **156**, 35 (1967).
[53]R. L. Martin and D. S. Shirley, J. Chem. Phys. **64**, 3685 (1976).
[54]P. Scott, A. E. Kingston, and A. Hibbert, J. Phys. B **16**, 3945 (1983).
[55]R. D. Cowan, J. E. Hansen, and H. Smid, Phys. Rev. A **31**, 2750 (1985).
[56]Z. Altun and H. P. Kelly, Phys. Rev. A **31**, 3711 (1985).
[57]J. E. Hansen and P. Scott, Phys. Rev. A **33**, 3133 (1986).